Quantum study of slow electron collisions with Rydberg atoms

S. X. Hu
Laboratory for Laser Energetics, University of Rochester, 250 E. River Road, Rochester, New York 14623
(Received 12 September 2006; published 27 December 2006)

Slow collisions of electrons with Rydberg sodium atoms have been quantum mechanically investigated by using the time-dependent close-coupling (TDCC) method. To make such large-scale calculations possible, it is essential to implement the TDCC method with the powerful finite-element discrete variable representation (FEDVR). Besides visualizing the slow collision dynamics, our quantum calculations show interesting features in the slow electron impact ionization of Rydberg atoms. The energy sharing between two continuum electrons changes dramatically as the incoming electron energy decreases. Predominant equal-energy sharing is observed in such a cold $(e,2e)$ process, even though the impact electron energy is still twice the binding energy of the Rydberg electron.

DOI: 10.1103/PhysRevA.74.062716 PACS number(s): 34.80.Dp, 34.60.+z

The accurate calculation of electron impact ionization of atoms as simple as hydrogen has been a long-standing difficult problem, even though quantum mechanics was founded more than 80 years ago. It was not completely solved until both time-independent and time-dependent numerical methods were developed in the past decade [1–4] with the aid of supercomputers. The difficulty lies in how well the electron correlation can be handled in such a three-body Coulomb system [5]. One direct way to fully account for three-body interactions is to nonperturbatively solve the time-dependent Schrödinger equation (TDSE). Time-dependent close coupling (TDCC) is such a method that uses partial wave expansions to effectively solve the TDSE for few-body systems [4]. It has been proven that TDCC calculations give the same results for three-body breakups as those from the time-independent methods [6]. However, the normal implementation of TDCC based on finite difference (FD) has limited its power to handle spatially extended problems such as electron impact ionization of highly excited atoms, although efforts using variable-mesh FD have been devoted to extending its capability [7]. It also turns out to be difficult for other methods to solve this problem of slow electron interactions with Rydberg atoms.

Slow collisions of electrons with Rydberg atoms is essentially important to better understand many physical processes that occur in astrophysics [8], frozen Rydberg gases [9], and ultracold plasmas [10], just to name a few. Although classical trajectory Monte Carlo methods have been applied to study electron collisions with Rydberg atoms for more than 30 yrs [11,12], fully quantal calculations are always sought not only to verify classical calculations or to justify the validity of semiclassical extrapolation from low-n data to high-n predictions, but also to reveal any potential quantum effects, especially in very low energy regimes. As the incoming electron energy decreases (longer de Broglie wavelength), one would expect that quantum effects such as Rydberg-state polarization and exchange interaction may become more important. In experiment, direct measurements of slow electron impact ionization of Rydberg atoms are now possible with advanced techniques. For example, a recent experiment [13] showed a large discrepancy with a previous theoretical prediction [14] and with a more recent semiclassical extrapolation [15]. These have motivated our efforts to extend the TDCC capability for quantum calculations of slow electron collisions with Rydberg atoms.

We have shown that the TDCC method can be perfectly implemented by using the finite-element discrete variable representation (FEDVR) [16]. The FEDVR-based TDCC method, which is easily parallelized on state-of-the-art supercomputers, has proven to be advantageous in accurately and efficiently solving spatially extended problems, such as the attosecond pump probe of electron wave packets within He atoms [17] and strong-field interactions with molecules [18]. In this paper, we further demonstrate its power by applying it to solve the hard computational problem in atomic physics: slow electron collisions with Rydberg atoms.

We consider slow collisions of Rydberg Na, which is initially in its $36s$ state, by free electrons having low energies of 0.05 eV or 0.025 eV (just a few times above the ionization threshold). To simulate the Coulomb interaction between a single electron with the Na^+ core, we have adopted an extensively used model potential [19]

$$V(r) = -\frac{1}{r}[Z_c + (Z - Z_c)e^{-a_1 r} + a_2 r e^{-a_3 r}] - \frac{\alpha_c}{2r^4}[1 - e^{-(r/r_c)^3}]^2, \tag{1}$$

with the empirical parameters: $a_1 = 3.324\,424\,5$, $a_2 = 0.713\,727\,9$, $a_3 = 1.832\,818\,2$, $\alpha_c = 0.9457$, and $r_c = 0.52\,4506\,3$, while the nuclear and core charges are $Z = 11$ and $Z_c = 1$, respectively. Diagonalizing the single electron Hamiltonian with this model potential in our FEDVR grid (discussed below), we obtain the eigenstates ϕ_{nl} of the Na atom. It gives a binding energy of $E_b = -0.0112$ eV for the $36s$ state ($n_0 = 36$), which agrees well with the accurate value of -0.0113 eV [20]. The incoming free electron is assumed to initially sit at a far distance ($r_0 \sim 3200$ bohr) away from the atomic core. It is described by a Gaussian wave pact [21]

$$G_{kl}(r) = \frac{(i)^l}{(\pi w^2)^{1/4}} e^{-(r - r_0)^2/2w^2} e^{-ikr}, \tag{2}$$

where $w = 400$ bohr is the width of the electron wave pact with a momentum k and l is its angular momentum quantum number. Thus, we can approximately express the total initial

state for such a collision system (LS symmetry) in a symmetrized product form of ϕ_{nl} and G_{kl}

$$\Psi^{LS}_{l_1 l_2}(r_1,r_2,t=0)=\frac{1}{\sqrt{2}}[\phi_{nl_1}(r_1)G_{kl_2}(r_2) + (-1)^S\phi_{nl_1}(r_2)G_{kl_2}(r_1)]. \quad (3)$$

The collision dynamics is governed by the fully six-dimensional (6D) TDSE, which has the following form (atomic units are used throughout):

$$i\frac{\partial}{\partial t}\Phi(\mathbf{r}_1,\mathbf{r}_2,t)=\left[-\frac{1}{2}(\Delta_{\mathbf{r}_1}+\Delta_{\mathbf{r}_2})+V(r_1)+V(r_2) + \frac{1}{|\mathbf{r}_1+\mathbf{r}_2|}\right]\Phi(\mathbf{r}_1,\mathbf{r}_2,t), \quad (4)$$

where $\mathbf{r}_1$ and $\mathbf{r}_2$ are the position vectors of each electron, with respect to the Na^+ core. We obtain a more tractable solution by following the time-dependent close-coupling (TDCC) recipe [4]: expanding the 6D wave function $\Phi(\mathbf{r}_1,\mathbf{r}_2|t)$ in terms of bipolar spherical harmonics $Y^{L,S}_{l_1 l_2}(\Omega_1,\Omega_2)$

$$\Phi(\mathbf{r}_1,\mathbf{r}_2|t)=\sum_{LS}\sum_{l_1 l_2}\frac{\Psi^{(LS)}_{l_1 l_2}(r_1,r_2|t)}{r_1 r_2}Y^{L,S}_{l_1 l_2}(\Omega_1,\Omega_2), \quad (5)$$

for a specific symmetry (LS). Also, we can expand the Coulomb repulsion term $1/|\mathbf{r}_1-\mathbf{r}_2|$ in terms of spherical harmonics. Substituting these expansions into the above Schrödinger Eq. (4) and integrating over angles Ω_1 and Ω_2 yields a set of coupled partial differential equations with only two radial variables, r_1 and r_2, left

$$i\frac{\partial}{\partial t}\Psi_j(r_1,r_2|t)=[\hat{T}_1+\hat{T}_2+\hat{V}_c]\Psi_j(r_1,r_2|t) + \sum_k \hat{V}^I_{j,k}(r_1,r_2|t)\Psi_k(r_1,r_2|t), \quad (6)$$

where the partial wave index j runs from 1 to the total number N of partial waves used for expansion. In Eq. (6), the diagonal operators $\hat{T}_1$, $\hat{T}_2$, and $\hat{V}_c$ give the kinetic energies and the Coulomb attractions between each electron and the Na^+ core, while the off-diagonal potential term $\hat{V}^I_{j,k}(r_1,r_2|t)$ consists of the Coulomb repulsion between the incident electron and the Rydberg electron.

Based on the FEDVR, we have generated an efficient time propagator with employing the real space product (RSP) algorithm. This sophisticated code (RSP-FEDVR) is parallelized in the scheme of message-passing interface (MPI), which has shown linear scaling up to ~500 CPU's on supercomputers (see details and its advantages in Ref. [16]). In calculations presented here, we have typically used 480 finite elements for each of the two radial dimension (r_1 and r_2), with a four-point basis within each element. The size of each finite element varies from the smallest value of 0.65 bohr to ~43.35 bohr outward, with an exponential factor of 4.2. With such an FEDVR setting, our grid spans a large space of ~4900 bohr in both r_1 and r_2 dimensions. The system is propagated in time until the collision process ends at t_f. To obtain the deexcitation and ionization probabilities, $P_e(nl,k_2)$ and $P_i(k_1,k_2)$, we need to perform the projection of the time-dependent wave packets onto bound or continuum states [22]

$$P_e(nl,k_2)=2\sum_{LS}(2L+1)(2S+1)\sum_{l_2}\left|\int\int dr_1 dr_2 \times \phi^*_{nl}(r_1)\phi^*_{k_2 l_2}(r_2)\Psi^{LS}_{l l_2}(r_1,r_2,t_f)\right|^2, \quad (7)$$

and

$$P_i(k_1,k_2)=2\sum_{LS}(2L+1)(2S+1)\sum_{l_1 l_2}|A_i(k_1 l_1,k_2 l_2,t_f)|^2 = 2\sum_{LS}(2L+1)(2S+1)\sum_{l_1 l_2}\left|\int\int dr_1 dr_2 \times \phi^*_{k_1 l_1}(r_1)\phi^*_{k_2 l_2}(r_2)\Psi^{LS}_{l_1 l_2}(r_1,r_2,t_f)\right|^2, \quad (8)$$

where ϕ_{nl} and ϕ_{kl} are the bound and continuum states, respectively. The continuum states ϕ_{kl} are obtained by diagonalizing the model potential [Eq. (1)] in our FEDVR grid. Integrating $P_e(nl,k_2)$ over k_2, we can obtain the probability of excitation or deexcitation to a specific state nl, that is, $P_e(nl)=\int P_e(nl,k_2)dk_2$. To see the energy-sharing information between the continuum electrons, we can define a energy differential probability as

$$\frac{dP_i}{dE_1}=2\sum_{LS}(2L+1)(2S+1)\int\int dk_1 dk_2\frac{1}{k_1 k_2} \times\delta\left[\alpha-\tan^{-1}\left(\frac{k_2}{k_1}\right)\right]\sum_{l_1,l_2}|A_i(k_1 l_1,k_2 l_2,t_f)|^2, \quad (9)$$

where the hyperspherical angle α defined in the k_1-k_2 plane describes the partition of excess energy, $E_{\mathrm{exc}}=\frac{k^2}{2}-|E_b|$, between two continuum electrons.

Although our FEDVR-based TDCC method has been successfully applied to (pump probe) photoionization of He [17] and strong-field interactions with molecules [18], we would verify its capability and accuracy to handle electron impact ionization problems before conducting the full-scale calculation of slow electron collisions with Rydberg atoms. For this purpose, we have applied our RSP-FEDVR code to calculate electron impact ionization of a ground-state hydrogen atom with an incident energy of 54.4 eV as used in Ref. [22]. We obtained excellent agreement between our calculation and those from both the FD-based TDCC computation and the time-independent ECS method [22]. We now turn to our large-scale calculations for the slow collisions of electrons with Rydberg Na ($36s$) atoms. Since we are considering very low incident electron energies of $E_i=0.05$ eV and $E_i=0.025$ eV, it is expected that the S-wave contribution would be dominant. Furthermore, as we can handle the collision by each total angular momentum configuration (LS) separately, we believe that calculations for high angular-momentum waves can be performed in the same fashion. Thus, we

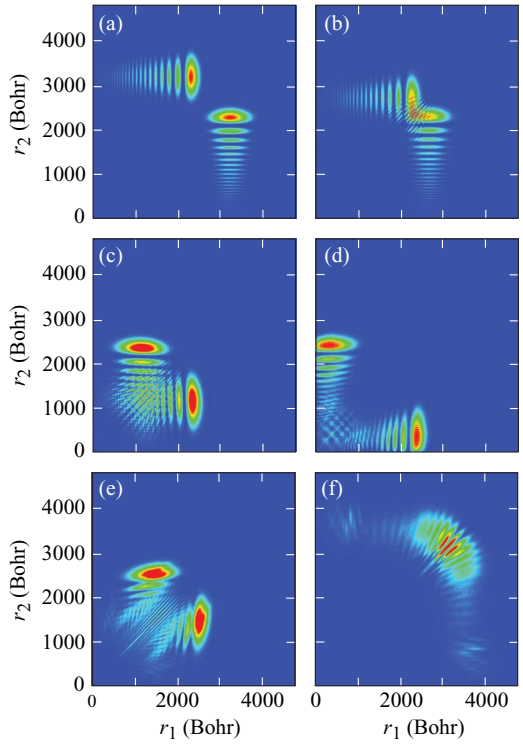

FIG. 1. (Color online) The snapshots of electron probability distribution on the plane spanned by the radial coordinates r_1 and r_2, for different times: (a) $t=0.0$ fs, (b) $t=200$ fs, (c) $t=800$ fs, (d) $t=1200$ fs, (e) $t=1600$ fs, and (f) $t=2400$ fs. The incident electron with an energy $E_i=0.05$ eV impacts on the Rydberg $(36s)$ Na atom.

present here our computations only for the S-wave case, i.e., $L=0(S=0)$ and $l_1=l_2=0-45$, in which a total of 46 partial waves are used for expansion. We have checked the convergence of our calculations and found little changes to our S-wave results by adding more partial waves.

To visualize the slow electron ($E_i=0.05$ eV) collision process, we have plotted in Fig. 1 the snapshots of electron probabilities $[\Sigma_j|\Psi_j(r_1,r_2,t)|^2]$ in the r_1r_2 plane for different times. We see that as the collision goes on, the two branches of electron probability (symmetric relative to the $r_1=r_2$ line) approach the Na^+ core (at the origin). It was illustrated that the Rydberg wave is gradually distorted during the slow collision [Figs. 1(c)–1(e)]. They reach to a minimum distance at $t=1200$ fs, as is shown in Fig. 1(d). Afterward, they "bounce" back to large r_1 and r_2 regions indicated in Figs. 1(e) and 1(f). The collision process tends to end at $t=2400$ fs. We therefore plot the electron probability in ln-scale in Fig. 1(f), to see clearly the deexcitation probabilities (the portion close to either r_1 or r_2 axis). We have also calculated the expectation values of $\langle p_{r_1}\rangle$ and $\langle r_1\rangle$ (same as $\langle p_{r_2}\rangle$ and $\langle r_2\rangle$ because the two electrons are indistinguishable), which are drawn as a function of the collision time in Fig. 2. We find that $\langle r_1\rangle$ reaches to a smaller minimum value in the case of $E_i=0.05$ eV when compared to that of the $E_i=0.025$ eV case (not shown here). This is reasonable because fast incident electrons can penetrate deeper into the Rydberg electron clouds.

At the end of collision $t_f=2400$ fs for $E_i=0.05$ eV (t_f

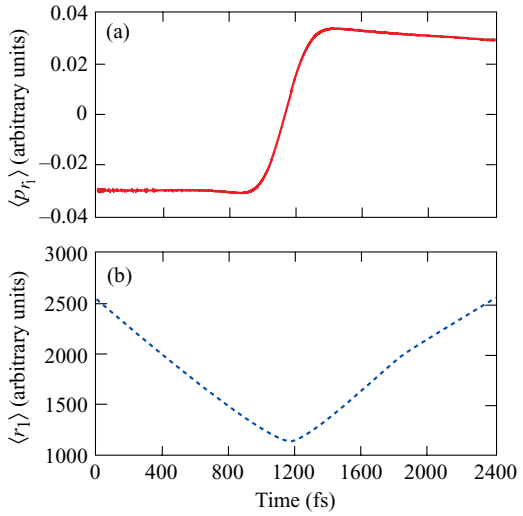

FIG. 2. (Color online) The calculated expectation values $\langle p_{r_1}\rangle$ and $\langle r_1\rangle$ as a function of the collision time, for the case shown in Fig. 1.

$=2900$ fs for $E_i=0.025$ eV), we estimated the probabilities for both deexcitation and ionization processes. The results are shown in Figs. 3 and 4. In Fig. 3(a), we plotted both the deexcitation $(n<n_0)$ and excitation $(n>n_0)$ probabilities $[P_e(n)]$ as a function of the quantum level n, by summing over all l sublevels. Unlike the case of fast electron collision, deexcitation and excitation of the Rydberg electron are much less significant than ionization in such slow collisions. We found that the total deexcitation probability is one order of magnitude less than that of ionization. The maximum n level

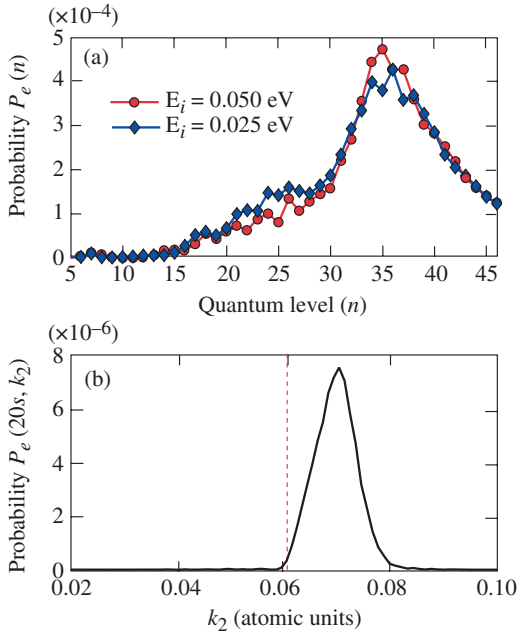

FIG. 3. (Color online) (a) The deexcitation and excitation probability $P_e(n)$ as a function of energy level n (summing over all l sublevels); (b) the deexcitation probability $P_e(20s,k_2)$ drawn against the outgoing electron momentum k_2. The dashed vertical line in (b) indicates the incident electron momentum.

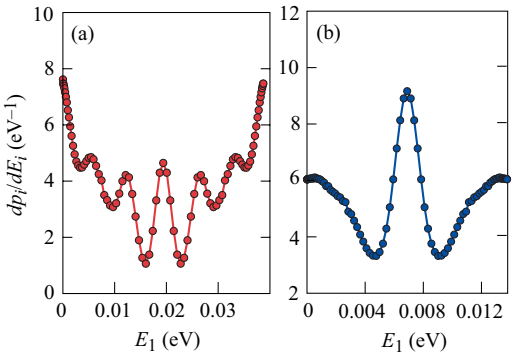

FIG. 4. (Color online) The energy-differential ionization probability of Rydberg Na (36*s*) *versus* the electron energy sharing for cases (a) E_i=0.05 eV and (b) E_i=0.025 eV.

is limited to n=46 for the box size we used. Generally, the excitation probability drops with n increasing, while the deexcitation ones exhibit oscillations against n. The similar deexcitation features are found for both incident electron energies. To further explore the three-body interaction dynamics, we draw the probability $P_e(nl,k_2)$ *versus* the outgoing electron momentum k_2 in Fig. 3(b) for the n_l=20*s* state. As we discussed above, $P_e(nl,k_2)$ is just the probability of one electron being deexcited or excited to nl level and the other electron being in the continuum with a momentum k_2. The dashed vertical line in Fig. 3(b) indicates the incident electron momentum. Figure 3(b) shows that when the Rydberg electron is deexcited from 36*s* to 20*s* state, the outgoing electron takes the excess energy $[\Delta E=E_b(36s)-E_b(20s)]$ so as to be speeded up in the continuum, which indicates the total energy conservation.

In Fig. 4, we plotted the energy-differential probability (dP_i/dE_1) for the electron impact ionization of the Rydberg Na (36*s*) atom in cases (a) E_i=0.05 eV and (b) E_i =0.025 eV, respectively. Integrating over E_1, we obtained a total ionization probability of 0.148 and 0.0729 for these two cases, respectively. The distinct feature of these figures is the oscillations of dP_i/dE_1, which is different from the smooth U shape in the case of fast electron impact ionization of ground-state atoms. Refining the grid setting in our FEDVR and increasing the number of partial waves in the expansion, we essentially found the same oscillations in the energy-differential ionization probability. This may be attributed to some intrinsic quantum effects: First of all, since the incoming electron is slowly approaching the target during the collision, the Rydberg atom can be easily polarized by the slow-impacting electron. Certain configuration of the polarized Rydberg electron clouds may favor or unfavor electron ejections for some specific energy sharing. Second, from the quantum-mechanics point of view, the slowly outgoing electron waves may continuously interfere with each other during the ionization process. Such interference can also result in the energy-sharing oscillations. Nevertheless, Fig. 4(a) still shows an overall U shape, although oscillations superpose on it. But when the incident electron energy further decreases to E_i=0.025 eV, a dramatic change is clearly seen in Fig. 4(b), where predominant equal-energy sharing occurs. It is noted that the incident electron energy E_i=0.025 eV is still twice the bind energy ($|E_b|$=0.0113 eV) of the Rydberg 36*s* electron, even though it looks very small. For the same condition ($E_i \sim 2|E_b|$), the fast electron impact ionization of ground-state atoms has given a totally different result: asymmetric energy sharing is most probable [22]. The dominant equal-energy sharing observed here is, therefore, unique for slow electron collision with Rydberg atoms.

In summary, we have quantum mechanically investigated the slow collisions of electrons with Rydberg atoms, using the time-dependent close-coupling method. To make such large-scale calculations possible, the FEDVR implementation of the TDCC method is essential, which enables the variable gridding but remains highly accurate. Our *S*-wave calculations show interesting oscillations in the energy-differential ionization probability of Rydberg atoms. Also, equal energy sharing was found to be predominant in such a slow $(e,2e)$ process, even though the incident electron energy is still twice the Rydberg binding energy. We expect that these predictions will motivate future experiments in this important field.

The author thanks Dr. Daniel Vrinceanu and Dr. Lee Collins for helpful discussions. This work was partially supported by the U.S. Department of Energy through Los Alamos National Laboratory.

[1] I. Bray and A. T. Stelbovics, Phys. Rev. Lett. **69**, 53 (1992).
[2] T. N. Rescigno *et al.*, Science **286**, 2474 (1999).
[3] K. Bartschat, S. Riordan, and G. Ver Steeg, Phys. Rev. A **65**, 060701(R) (2002).
[4] M. S. Pindzola and F. Robicheaux, Phys. Rev. A **54**, 2142 (1996).
[5] J. S. Briggs and V. Schmidt, J. Phys. B **33**, R1 (2000); G. Tanner, K. Richter, and J.-M. Rost, Rev. Mod. Phys. **72**, 497 (2000).
[6] D. A. Horner, J. Colgan, F. Martin, C. W. McCurdy, M. S. Pindzola, and T. N. Rescigno, Phys. Rev. A **70**, 064701 (2004).
[7] M. Witthoeft, J. Colgan, M. S. Pindzola, C. P. Ballance, and D. C. Griffin, Phys. Rev. A **68**, 022711 (2003).
[8] J. W. Ferguson and G. J. Ferland, Astrophys. J. **479**, 363 (1997).
[9] M. P. Robinson, B. LaburtheTolra, M. W. Noel, T. F. Gallagher, and P. Pillet, Phys. Rev. Lett. **85**, 4466 (2000).
[10] T. C. Killian, S. Kulin, S. D. Bergeson, L. A. Orozco, C. Orzel, and S. L. Rolston, Phys. Rev. Lett. **83**, 4776 (1999).
[11] I. C. Percival, J. Phys. B **6**, 93 (1973); R. E. Olson and A. Salop, Phys. Rev. A **16**, 531 (1977).
[12] D. Vrinceanu, Phys. Rev. A **72**, 022722 (2005).
[13] K. Nagesha and K. B. MacAdam, Phys. Rev. Lett. **91**, 113202

(2003).
[14] L. Vriens and A. H. M. Smeets, Phys. Rev. A **22**, 940 (1980).
[15] H. Deutsch *et al.*, J. Phys. B **39**, 343 (2006).
[16] B. I. Schneider, L. A. Collins, and S. X. Hu, Phys. Rev. E **73**, 036708 (2006).
[17] S. X. Hu and L. A. Collins, Phys. Rev. Lett. **96**, 073004 (2006).
[18] S. X. Hu and L. A. Collins, Phys. Rev. A **73**, 023405 (2006); S. X. Hu and L. A. Collins, J. Phys. B **39**, L185 (2006).
[19] C.-N. Liu and A. F. Starace, Phys. Rev. A **59**, 3643 (1999).
[20] NIST, NIST Atomic Spectra Database, NIST Standard Reference Database #78, 1999, http://physics.nist.gov/cgi-bin/AtData/main_asd.
[21] W. Ihra, M. Draeger, G. Handke, and H. Friedrich, Phys. Rev. A **52**, 3752 (1995); D. M. Mitnik, D. C. Griffin, and M. S. Pindzola, Phys. Rev. Lett. **88**, 173004 (2002).
[22] J. Colgan, M. S. Pindzola, F. J. Robicheaux, D. C. Griffin, and M. Baertschy, Phys. Rev. A **65**, 042721 (2002).